Please cite the Published Version

Damage degradation modelling for transverse cracking in composite laminates under low-velocity impact

Ghalib R. Ibrahim [a,b,*], A. Albarbar [a], Khaldoon F. Brethee [b]

[a] *Smart Infrastructure and Industry Research Group, Department of Engineering, Manchester Metropolitan University, Manchester M1 5GD, UK*
[b] *Mechanical Engineering Department, College of Engineering, University of Anbar, Anbar, Iraq*

ARTICLE INFO

ABSTRACT

This paper derives a damage evaluation law for fibres and an expression for the damage parameter function. It also proposes an approach to the matrix damage degradation law. A proposed approach to both the constitutive damage degradation model and increment law is developed to predict intralaminar damage evolution in composite laminates. Failure envelopes for different failure criteria are discussed in term of the fracture plane of matrix cracking under compressive load. The damage surface consistency condition is applied to derive a plastic multiplier as a function of the damage plastic flow so that the plastic strain is updated at each time increment and the stress–strain constitutive relationship of the damage model will also be updated. A user-defined subroutine has been adopted to implement a proposed constitutive damage degradation model. The effectiveness of the proposed method has been examined under low velocity impact. The numerical findings confirm that results obtained using the suggested approach are in good agreement with experimental results.

1. Introduction

Materials of high stiffness-to-weight ratio, strength-to-weight ratio, and resistance to fatigue failure should be chosen for structure manufacturer e.g. aeroplane and wind turbine blades etc. While composite laminates formally meet the requirements, damage incurred due to foreign objects, e.g. heavy sands, birds, etc., impacting on the structures. All damage types start as unseen cracks and develop as one or more damage modes e.g. matrix cracking, fibre breakage, and/or delamination, all of which can lead to catastrophic failure of the structure [32].

An impact load on the composite materials can be more dangerous than on metals components because the defect is undetectable by the naked eye. Investigations to assess the damage behaviour of composite structures subjected to impact loads are not a recent development. Composite structures used in aerospace and defence applications and, more recently, the issue of lifted offshore wind blade have been examined by many researchers. The damage develops in the structures due to impact by an external object e.g. birds, or during installation when the wind blades are lifted from the ship or ground to the hub [28].

Numerical simulation is an effective tools to analyse fibre reinforced polymer composites, and computational simulation of intralaminar and interlaminar damage is considered a powerful and fast tool compared to experimental tests [26]. Much research has been undertaken in this field see, for example, the finite element analyses presented by Turon et al. [27], Donadon et al. [3], Aymerich and Priolo [1], Yang et al. [30], Haselbach et al. [9], Fagan et al. [5] to investigate progressive damage modes.

---

* Corresponding author.

Liu et al. [17] used various failure criteria, e.g. Puck, Hashin and Chang–Chang, to investigate how well they modelled dynamic progressive failure of laminated composites. Their investigation showed that, compared to the other two, the Puck criteria had some advantages when predicting failure, but was limited regarding accurate determination of the angle of the fracture plane. Shor and Vaziri [22] used local cohesive zone (LCZ) method of progressive delamination in large-scale laminated composite. Two dynamic models, tubes axial crushing and transverse impact loading of plates, were investigated. Their results were compared to the conventional cohesive zone method and available experimental data. The results showed that the LCZ algorithm can adaptively split the structural elements through-thickness during the tubes axial crushing process.

Namdar and Darendeliler [18] investigated buckling, post-buckling and progressive failure of laminated plates numerically and experimentally. The 2D Hashin failure criteria was used to model intra-laminar damage in the laminated plates. The results indicated that the stacking sequence and the ply thickness affected the buckling, and failure progression.

Tan et al. [25] investigated the effect of matrix cracking on developing delamination in laminated composites. The extended finite element method (XFEM) and the Puck criteria were adopted by the authors to predict matrix cracking. Their findings showed that the matrix crack in the bottom layer contributed to narrow delamination in the region beneath the impact location. Wu et al. [29] studied the transverse low-velocity impact response and residual axial compression behaviour of braided composite tube. They carried out experimentally and numerically quasi-static axial compression of intact and pre-damaged tubes. The effects of wall thickness on the mechanical response were investigated by authors. The finite element model demonstrated that the proposed model can capacity to capture damage variables due to transverse impact in the axial compression process.

Jiang et al. [15] used quasi-static and fatigue tests under various load conditions (stress levels) of cross-ply glass fibre reinforced plastic (GFRP) laminates. Their studies focused on the stiffness degradation curves and matrix damage evolution. It was observed that the fracture dimension evolution of transverse damage could be divided into three stages: (I) an initial slow rise, (II) a rapid rise, and (III) a final slow rise. Sridharan and Pankow [23] presented two progressive damage model and investigated them in the commercial finite element software which is Abaqus/CAE and LS-Dyna. They used VUMAT subroutine of the Abaqus/CAE and MAT 162 of LS-Dyna. Their study was carried out on composite laminates subject to both low velocity and high-velocity projectile. In general, the findings showed models are able to accurately predict the damage in the composite laminates subjected to low and high velocities. Their results showed that Abaqus/CAE has good correlation with experimental for low velocity thicker laminates while MAT 162 can capture ballistic limits of high-velocity projectiles.

Donadon et al. [3] introduced damage propagation laws as a function of strains with their failure initiation strain and maximum strain either in tension or compression. The critical values of strain (initiation and failure strain) are defined as a function of the fracture energies damaged material. The progressive damage parameter laws to predict transverse cracks and fiber failure whether composite laminates subjected to tension or compression were proposed by authors as described below;

$$d_i = \frac{\varepsilon_i^f}{\varepsilon_i^f - \varepsilon_i^o} \left(1 - \frac{\varepsilon_i^1}{\varepsilon_i}\right) \tag{1}$$

where $i = 1$ indicates longitudinal direction (fiber), $i = 2$ represents transverse direction (matrix). ε_i^f is failure strain when the shear stress equals zero and ε_i^o is strain at initiation point. Rivallant et al. [20] used linear damage degradation of softening region for both matrix and fiber damage based on strain or displacement. The cohesive elements were used to simulate intra-ply matrix cracking and delamination based on linear damage evaluation law. Fakoor and Ghoreishi [6] presented a modified method for damage evolution of composite laminates so that can predict a reduction of ply stiffness whether the matrix and fiber stiffness reduction occur gradually or suddenly. The authors proposed an exponential progressive damage model of the softening part in the damaged ply which is written in the equation below. The exponent α in their proposed formula represents the softening rules with different behaviour so that if the $\alpha = 0$, the linear material softening will take place. While the sudden degradation will occur when the exponent goes to infinity ($\alpha = \infty$).

$$d = \frac{1 - e^{-(\alpha+1)\left(\frac{\delta_{eq} - \delta_{eq}^0}{\delta_{eq}^f - \delta_{eq}^0}\right)}}{1 - e^{-(\alpha+1)}} \tag{2}$$

δ_{eq}^0 is the equivalent displacement at damage initiation. δ_{eq}^f represents the final displacement when full damage has taken place in the ply. The exponent α of the damaged ply is determined by comparing the simulation results with experimental results. Therefore, it is considered a negative point of this equation.

A literature review has confirmed that many studies have experimentally investigated the effect of intralaminar damage in laminated composites. However, few studies have simulated a damage degradation model and the incremental damage law under different load conditions (tension, compression, and shear) despite extensive computational simulation is necessary to replace experimental test time and cost. This paper presents a developed model to assess damage degradation of matrix and fibres and takes into consideration the load condition. A new approach to the damage evaluation law for matrix, fibres and shear failure is derived based on the damage surface concept [14].

2. Intralaminar yield surface criteria

The yield surface behaviour in the laminated composite can be determined using strength-based yield criteria. Various failure criteria have been widely employed to predict the damage initiation in the composite structure. Hashin and Rotem [11] and Hashin
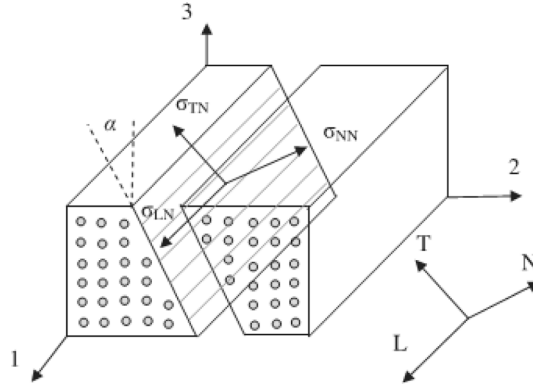
Fig. 1. Fracture plane of matrix cracking under compressive load [21].

[10] confirmed the need for failure criteria that are based on failure mechanisms and proposed a yield surface criterion based on their experimental observations made during tensile tests. Two failure criteria were introduced to indicate the damage in the fibre and matrix. Quadratic failure criteria were presented to include the stresses interaction that acting on the failure plane. The Hashin failure criteria are written as follows [10]:

Fibre tension damage initiation ($\sigma_{11} > 0$);

$$\left(\frac{\sigma_{11}}{X_T}\right)^2 \geq 1 \tag{3}$$

Fibre compression damage initiation ($\sigma_{11} < 0$);

$$\left(\frac{\sigma_1}{X_C}\right)^2 \leq 1 \tag{4}$$

Matrix tension damage initiation ($\sigma_{22} > 0$);

$$\left(\frac{\sigma_{22}}{Y_T}\right)^2 + \left(\frac{\sigma_{12}}{S_{12}}\right)^2 \geq 1 \tag{5}$$

Matrix compression damage initiation ($\sigma_{22} < 0$)

$$\left(\frac{\sigma_{22}}{Y_C}\right)^2 + \left(\frac{\sigma_{12}}{S_{12}}\right)^2 \leq 1 \tag{6}$$

where σ_{11} is the stress in the direction of the fibres, σ_{22} is the stress in the transverse direction perpendicular to the fibres, X_T is the tensile strength and X_C is the compressive strength of the fibres, Y_T is the tensile strength and Y_C is the compressive strength of the matrix. σ_{12} and S_{12} are the shear stress and transverse shear strength respectively [8].

Many studies have investigated the effectiveness of Hashin's criterion especially in the case of the compression mode. The experimental data indicates that the weakness of Hashin's criterion is its sensitivity to the onset of failure when the laminated composite undergoes compressive load. Experimental evidence has demonstrated that the shear strength of a ply increases when the unidirectional laminates are subjected to moderate transverse compression ($\sigma_{22} < 0$), [2].

Many modifications have been made to improve the Hashin criteria's predictive capabilities. Sun et al. [24] introduced an empirical modification to matrix cracking failure under compressive load, they modified Hashin's criteria to take into consideration the increase in shear strength due to compressive stress ($\sigma_{22} < 0$). This modification is written as;

$$\left(\frac{\sigma_{22}}{Y_C}\right)^2 + \left(\frac{\sigma_{12}}{S_{12} + \mu\sigma_{22}}\right)^2 = 1 \tag{7}$$

where μ is a constant found experimentally, it plays a role similar to a friction coefficient and is referred as an internal material friction parameter. The denominator of the modified criterion ($S_{12} + \mu\sigma_{22}$) increases the effective longitudinal shear strength when transverse compression occurs.

Puck and Schürmann [19] experimentally studied unidirectional composite laminate under transverse compression. Their investigation focused on the fracture plane orientation due to matrix compression. The experimental findings showed that the transverse damage occurred when shear stress along fracture plane was oriented by an angle $\alpha = 53 \mp 2^0$ with respect to the fibre orientation. The angle of the fracture plane, α, is illustrated in Fig. 1, which also shows the three stress transformations (L. T and N) which act on the fracture plane [3,16].

In order to take these features into consideration, the failure theory adopted should include the combination of the three stress transformations in the fracture plane. Puck and Schürmann [19] introduced a solution based on the Mohr-Coulomb failure criterion,
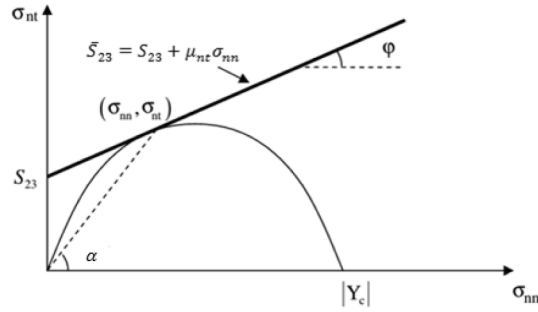
Fig. 2. Tangential line of Mohr–Coulomb behaviour for transverse compression [3].
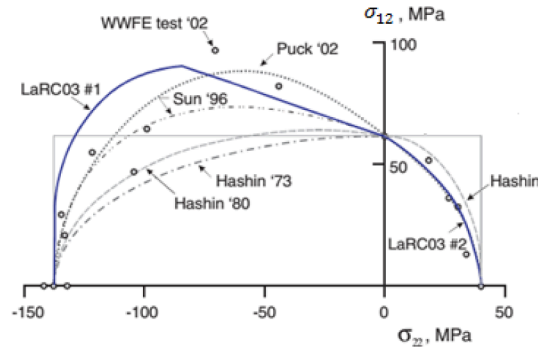

Fig. 3. Failure envelopes of the various failure criteria [2].

and a local quadratic stress interaction was suggested to determine onset of the failure. In their modifications, normal compressive stress (σ_{nn}), shear stress (σ_{nt}) and (σ_{nl}) which act together on the fracture plane should be taken into consideration and compared with the strengths in their action planes.

The second suggestion presented by Puck and Schürmann [19] assumed that the transverse compressive stress on the yield surface plane affects failure initiation and enhances the resistance to shear fracture. Fig. 2 shows how out-of-plane shear strength (S_{23}) and in-plane shear strength (S_{12}) can be enhanced as functions of the normal compressive stress (σ_{nn}). The tangent to the Mohr–Coulomb curve for transverse compression, shown in Fig. 2, is typically expressed by the equation of a line ($\bar{S}_{23} = S_{23} + \mu_{nt}\sigma_{nn}$), where the intercept point on the σ_{nt} axis is transverse shear strength S_{23}, and the gradient of the line is $\mu_{nt} = \tan(\varphi)$, where $\varphi = 2\alpha - 90$. Therefore, resistance to shear fracture increases as a function of the normal compressive stress. Similarly, ($\bar{S}_{12} = S_{12} + \mu_{nl}\sigma_{nn}$) for in-plane shear strength (S_{12}). The proposed fracture failure criterion of Puck and Schürmann [19] can be written as;

$$\mathscr{F}_{22}^c(\sigma_{nt}, \sigma_{nl}, \bar{S}_{12}, \bar{S}_{23}) = (\frac{\sigma_{nl}}{\bar{S}_{12}})^2 + (\frac{\sigma_{nt}}{\bar{S}_{23}})^2 \geq 1 \tag{8}$$

Substituting for $\bar{S}_{12}$ and $\bar{S}_{23}$, the failure criterion for transverse compression failure can be written as;

$$\mathscr{F}_{22}^c(\sigma_{nn}, \sigma_{nt}, \sigma_{nl}) = (\frac{\sigma_{nl}}{S_{12} + \mu_{nl}\sigma_{nn}})^2 + (\frac{\sigma_{nt}}{S_{23} + \mu_{nt}\sigma_{nn}})^2 \geq 1 \tag{9}$$

3. Derivation of damage degradation model and incremental law

The experimental tests carried out as part of the World-Wide Failure Exercise (WWEF) for predicting failure in composite laminates [12] compared failure results predicted by the failure criteria for unidirectional composite E-Glass/LY556 with experimental evidence to investigate the strengths and weaknesses of each of the criteria. Fig. 3 presents the failure envelopes of the various failure criteria together with experimental results over the transverse stress (σ_{22}) – shear stress (σ_{12}) domain to identify the overall effectiveness of each theory. It can be observed that in the tension test (positive range of σ_{22}) all failure criteria predictions of the yield surface are close to the experimental data (WWEF test) performed by Hinton et al. [12]. In the compression test, the failure criteria should be carefully selected to determine the onset of the failure. The boundary of the failure envelope obtained by Hashin and Rotem [11] when σ_{22} has a negative sign (compressive) does not fit experimental data. Hashin [10] presented a modest improvement in accuracy of the predicted failures, and the failure behaviour was closer to the experimental results as shown in Fig. 3. However, the modified failure criteria by Sun et al. [24] and Puck and Schürmann [19] gave more satisfactory results and showed significant improvement compared with Hashin's criteria.
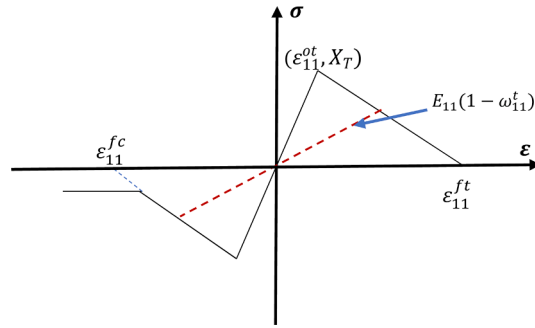
Fig. 4. Damage behaviour in the fibre direction.

If damage in the composite laminates takes place, it is very important to understand how the stiffness of the material is degraded by the damage mode. The concept of damage evolution assumes that material failure will follow an ongoing reduction in the stiffness of the material [8]. Damage evolution laws or rules are used for describing the failure propagation in the structure.

Stress or strain-based failure criteria have been used by many researchers to assess the damage level in laminated composites. The four major damage degradation modes in laminated composites are: matrix tension, matrix compression, fibre tension and fibre compression damage, in addition to which this paper introduces shear damage degradation as a new approach. For simplicity, damage propagation behaviour will be developed based on Hashin and Rotem [11] when laminated composites were subjected to tensile or transverse compressive stresses.

The new approach to the damage evaluation law can be derived based on the damage surface concept [14]. The damage surface is written as:

Initiation criteria ($\mathbb{F}_i$) + Propagation criteria (Ψ) = 1

The undamaged specimen is assumed linearly elastic, see Fig. 4, this is followed by the onset of damage, whether transverse cracking damage or fibre breakage can be determined by using one of the above-mentioned failure criteria. As shown in Fig. 4, it is clearly observed that the strain, ε_{11}^{ft} and ε_{11}^{fc} represent the maximum values of strain when the damage parameter reaches unity in tension and compression tests, respectively. Also, it can be noticed the longitudinal direct stress σ_{11} is degraded according to $\sigma_{11} = E_{11}(1 - \omega_{11})\varepsilon_{11}$ until complete failure of an element takes place in tension, or approaches a minimum residual strength which is comparable to the transverse compressive strength [3,7,17].

The damage evolution law of each damage mode for fibre or matrix is achieved in this study using damage initiation and surface concepts. The damage initiation of the fibre was introduced by Hashin and Rotem [11] as ($\sigma_{11} > 0$) and ($\sigma_{11} < 0$) these are substituted in the damage surface as;

$$\left(\frac{\sigma_{11}}{X_T}\right)^2 + \Psi_{11}^t = 1 \quad \sigma_{11} > 0 \tag{10}$$

$$\left(\frac{\sigma_{11}}{X_C}\right)^2 + \Psi_{11}^c = 1 \quad \sigma_{11} < 0 \tag{11}$$

where Ψ_{11} is the damage growth function which depends on energy release rate (G_{11}) during loading and unloading, and fracture toughness [13]. Damage growth under pure-mode loading based on energy release rate during loading, and fracture toughness [14], is written as;

$$\Psi_{11}^t = \frac{G_{11}}{G_{f11}^t} \quad \sigma_{11} > 0 \tag{12}$$

$$\Psi_{11}^c = \frac{G_{11}}{G_{f11}^c} \quad \sigma_{11} < 0 \tag{13}$$

where G_{f11}^t, G_{f11}^c are intralaminar fracture toughness in tension and compression respectively with respect to the direction of the fibres.

The damage parameter symbol of a fibre under tension and compression is written in this study as ω_{11}^t, and ω_{11}^c respectively. Therefore, the stress will be degraded for both load conditions (tension and compression) as follows;

$$\sigma_{11} = E_{11}(1 - \omega_{11}^t)\varepsilon_{11}^t \quad \sigma_{11} > 0 \tag{14}$$

$$\sigma_{11} = E_{11}(1 - \omega_{11}^c)\varepsilon_{11}^c \quad \sigma_{11} < 0 \tag{15}$$

where E_{11} is longitudinal Young's modulus, ε_{11}^t and ε_{11}^c are tension and compression strains in the direction of the fibres.

Substituting the longitudinal direct stress (σ_{11}) degradation into the damage surface and re-arranging the equations, we derive the

new damage evaluation law for fibres. The new damage parameter function is written as;

$$\omega_{11}^t = 1 - \left(\frac{X_T}{E_{11}\varepsilon_{11}^t}\right)\sqrt{1 - \Psi_{11}^t} \quad \sigma_{11} > 0 \tag{16}$$

$$\omega_{11}^c = 1 - \left(\frac{X_C}{E_{11}\varepsilon_{11}^c}\right)\sqrt{1 - \Psi_{11}^c} \quad \sigma_{11} < 0 \tag{17}$$

The second goal of this paper is to determine a new approach to the matrix damage degradation law. The failure criteria of the matrix damage initiation introduced by Hashin and Rotem [11] when ($\sigma_{22} > 0$) is substituted in the damage surface as;

$$\left(\frac{\sigma_{22}}{Y_T}\right)^2 + \left(\frac{\sigma_{12}}{S_{12}}\right)^2 + \Psi_{22}^t = 1 \tag{18}$$

The stress (σ_{22}) in the transverse direction is assumed to degrade as $\sigma_{22} = E_{22}(1 - \omega_{22}^t)\varepsilon_{22}^t$. Where ω_{22}^t is the matrix damage parameter under tension, ε_{22}^t is the tension strain in the transverse direction, and E_{22} is the transverse Young's modulus. The propagation failure criteria of the tension matrix cracking, Ψ_{22}^t, is written as;

$$\Psi_{22}^t = \frac{G_{22}}{G_{m22}^t} \tag{19}$$

where G_{m22}^t is the intralaminar fracture toughness in tension in the transverse direction, and G_{22} is energy release rate during matrix cracking.

When the transverse stress degradation is substituted in the damage surface condition, the equation can be written as;

$$\left(\frac{E_{22}(1 - \omega_{22}^t)\varepsilon_{22}^t}{Y_T}\right)^2 + \left(\frac{\sigma_{12}}{S_{12}}\right)^2 + \Psi_{22}^t = 1 \tag{20}$$

The new approach to the damage evolution law for matrix cracking in tension is developed as;

$$\omega_{22}^t = 1 - \left(\frac{Y_T}{E_{22}\varepsilon_{22}^t}\right)\sqrt{1 - \left(\frac{\sigma_{12}}{S_{12}}\right)^2 - \Psi_{22}^t} \tag{21}$$

The failure criteria introduced by Hashin and Rotem [11] is also adopted to develop the damage degradation law when a compressive load is applied ($\sigma_{22} < 0$). It is useful to mention that the stress (σ_{22}) in the transverse direction under compression is degraded as $\sigma_{22} = E_{22}(1 - \omega_{22}^c)\varepsilon_{22}^c$. So that ω_{22}^c is the matrix damage parameter under a compressive load, and ε_{22}^c is compression strain in the transverse direction. The damage surface for matrix cracking under compression is written as;

$$\left(\frac{\sigma_{22}}{Y_C}\right)^2 + \left(\frac{\sigma_{12}}{S_{12}}\right)^2 + \Psi_{22}^c = 1 \tag{22}$$

The propagation criteria of transverse matrix cracking under compression is Ψ_{22}^c, is written as;

$$\Psi_{22}^t = \frac{G_{22}}{G_{m22}^c} \tag{23}$$

where G_{m22}^c is intralaminar fracture toughness in compression for the transverse direction of the compressive load.
The stiffness degradation is determined based on the damage surface condition as;

$$\left(\frac{E_{22}(1 - \omega_{22}^c)\varepsilon_{22}^c}{Y_C}\right)^2 + \left(\frac{\sigma_{12}}{S_{12}}\right)^2 + \Psi_{22}^c = 1 \tag{24}$$

The new damage evolution law of matrix cracking under compressive load is now developed as;

$$\omega_{22}^c = 1 - \left(\frac{Y_C}{E_{22}\varepsilon_{22}^c}\right)\sqrt{1 - \left(\frac{\sigma_{12}}{S_{12}}\right)^2 - \Psi_{22}^c} \tag{25}$$

It is important to determine the incremental damage constitutive relationship for each damage scenario. The incremental form of the relationship between strain and damage parameter can be obtained for the fibre and matrix using an infinitesimal change in the condition of the damage surface. The procedure below is adopted to consider incremental damage due to matrix cracking under tension load ($\sigma_{22} > 0$).

The criteria for the onset of failure and damage propagation can be written as;

$$F_s = \left(\frac{\sigma_{22}}{Y_T}\right)^2 + \left(\frac{\sigma_{12}}{S_{12}}\right)^2 - 1 = 0 \quad \text{(Damage initiation)} \tag{26}$$

$$\Pi_g = \Psi - 1 = 0 \quad \text{(Damage propagation)} \tag{27}$$

Therefore, the damage surface can be written as;

$$\mathscr{F}(\sigma, \Psi) = F_s + \Pi_g - 1 \tag{28}$$

The incremental damage evolution law can be determined based on the consistency condition, $\dot{\mathscr{F}} = 0$, [13] as;

$$\frac{\partial F_s}{\partial \sigma_{22}}(\partial \sigma_{22}) + \frac{\partial F_s}{\partial \sigma_{12}}(\partial \sigma_{12}) + \frac{\partial \Pi_g}{\partial \Psi} \partial \Psi = 0 \tag{29}$$

So that,

$$\partial \sigma_{22} = E_{22}\left(1 - \omega_{22}^t\right)\partial \varepsilon_{22}^t - E_{22}\varepsilon_{22}^t\left(\partial \omega_{22}^t\right) \tag{30}$$

The stress (σ_{12}) in the plane 12 is assumed to degrade as $\sigma_{12} = G_{12}(1 - \omega_{12})\varepsilon_{12}$, therefore ($\partial \sigma_{12}$) is determined as;

$$\partial \sigma_{12} = G_{12}(1 - \omega_{12})\partial \varepsilon_{12} - G_{12}\varepsilon_{12}(\partial \omega_{12}) \tag{31}$$

where ω_{12} is the damage evolution in plane 12, due to the in-plane shear stress. The maximum shear stress criterion is adopted here as the damage criterion for shear failures to determine shear damage degradation.

Shear failures is $\left(\frac{\sigma_{12}}{S_{12}}\right)^2 \geq 1 \tag{32}$

The shear failure criteria of damage initiation in plane 12 is substituted in the damage surface as;

$$\left(\frac{\sigma_{12}}{S_{12}}\right)^2 + \Psi_{12} = 1 \tag{33}$$

By substituting, $\sigma_{12} = G_{12}(1 - \omega_{12})\varepsilon_{12}$, in above equation, the stiffness degradation is determined based on the damage surface condition as;

$$\left(\frac{G_{12}(1 - \omega_{12})\varepsilon_{12}}{S_{12}}\right)^2 + \Psi_{12} = 1 \tag{34}$$

Therefore, the new damage evolution law of shear stress can be expressed as;

$$\omega_{12} = 1 - \left(\frac{S_{12}}{G_{12}\varepsilon_{12}}\right)\sqrt{1 - \Psi_{12}} \tag{35}$$

and new damage degradation increment ($\partial \omega_{12}$) is Witten as;

$$\partial \omega_{12} = \frac{(1 - \omega_{12})}{\varepsilon_{12}}\partial \varepsilon_{12} \tag{36}$$

where G_{12}, ε_{12} represent shear moduli and shear strain, respectively, in plane 12.

Π_g is assumed to be a constant for each increment and is updated at the end of the current increment. According to this assumption $\frac{\partial \Pi_g}{\partial \Psi}$ equals zero, so the incremental damage constitutive relationship can now be expressed as;

$$\frac{\partial \omega_{22}^t}{\partial \varepsilon_{22}^t} = \frac{\frac{\partial F_s}{\partial \sigma_{22}}\left(E_{22}\left(1 - \omega_{22}^t\right)\partial \varepsilon_{22}^t\right) + \frac{\partial F_s}{\partial \sigma_{12}}(G_{12}(1 - \omega_{12})\partial \varepsilon_{12}) - \frac{\partial F_s}{\partial \sigma_{12}}(G_{12}\varepsilon_{12}(\partial \omega_{12}))}{\frac{\partial F_s}{\partial \sigma_{22}}\left(E_{22}\varepsilon_{22}^t(\partial \omega_{22}^t)\right)} \tag{37}$$

The same procedure can be followed to develop a new approach to the incremental damage evolution law for matrix cracking under compressive load as well as incremental damage of the fibre.

- incremental damage for matrix cracking ($\sigma_{22} < 0$)

$$\frac{\partial \omega_{22}^c}{\partial \varepsilon_{22}^c} = \frac{\frac{\partial F_s}{\partial \sigma_{22}}\left(E_{22}\left(1 - \omega_{22}^c\right)\partial \varepsilon_{22}^c\right) + \frac{\partial F_s}{\partial \sigma_{12}}(G_{12}(1 - \omega_{12})\partial \varepsilon_{12}) - \frac{\partial F_s}{\partial \sigma_{12}}(G_{12}\varepsilon_{12}(\partial \omega_{12}))}{\frac{\partial F_s}{\partial \sigma_{22}}\left(E_{22}\varepsilon_{22}^c(\partial \omega_{22}^c)\right)} \tag{38}$$

- incremental damage of fibre ($\sigma_{11} < 0$)

$$\frac{\partial \omega_{11}^c}{\partial \varepsilon_{11}^c} = \frac{1 - \omega_{11}^c}{\varepsilon_{11}^c} \tag{39}$$

- incremental damage of fibre ($\sigma_{11} > 0$)

$$\frac{\partial \omega_{11}^t}{\partial \varepsilon_{11}^t} = \frac{1 - \omega_{11}^t}{\varepsilon_{11}^t} \tag{40}$$

Donadon et al. [3], Feng and Aymerich [7], and Liu et al. [17] adopted damage evaluation law for fibres and matrix as ($d(\varepsilon) = \varepsilon_{failure}(1 - \frac{\varepsilon_{initiation}}{\varepsilon})/(\varepsilon_{failure} - \varepsilon_{initiation})$) and incremental damage as $\Delta d(\varepsilon) = \varepsilon_{failure}(\frac{\varepsilon_{initiation}}{\varepsilon^2})/(\varepsilon_{failure} - \varepsilon_{initiation})\Delta \varepsilon$. It is clearly seen both
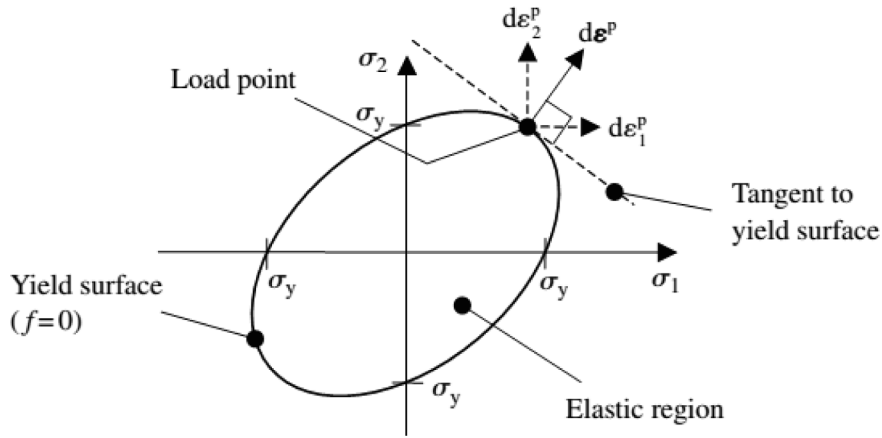
Fig. 5. Plastic strain increment based on von Mises theory [4].

damage evaluation law and its incremental are a function of strain during the iterations in each increment. This leads sometimes to severe convergence problems that are often encountered during the non-linear solution procedure of some complicated case study. Therefore, to overcome on convergence problem in numerical simulation, the proposed damage evolution law of each damage mode for fibre or matrix takes into account damage growth function which depends on energy release rate during loading /unloading, and fracture toughness as well as the displacement (strain). In addition, damage evolution law for matrix includes the shear stress in plane 12. Also, incremental damage for matrix cracking is a function of the rate of damage initiation, strain, shear moduli, and shear while incremental damage that was adopted [3,7,17] is just a function of strain so sometimes the numerical solution faces convergence problems. Consequently, it is more sensitive to incremental damage and has more accurate predictions.

4. Hypotheses of plasticity model

The direction of flow (damage propagation) can be determined based on the normality hypothesis of plasticity. In this hypothesis, the plastic strain tensor grows perpendicular to the tangent to the yield surface at the load point as shown in Fig. 5 which represents the von Mises yield surface for isotropic plane stress.

The failure functions mentioned in the previous section has been adopted here to determine the increment in the plastic strain tensor $d\varepsilon^p$. By using the associated flow rule, the plastic strain can be written in terms of the failure criteria (yield function) as;

$$d\pmb{\varepsilon}^p = d\lambda \frac{\partial F_s}{\partial \pmb{\sigma}} \tag{41}$$

while the plastic strain rate ($\dot{\varepsilon}^p$) can be expressed as;

$$\dot{\pmb{\varepsilon}}^p = \dot{\lambda} \frac{\partial F_s}{\partial \pmb{\sigma}} \tag{42}$$

where $d\lambda$ is the plastic multiplier, $\frac{\partial F_s}{\partial \sigma}$ is determining the direction of plastic flow, and F_s is the yield criterion which is used here as the plastic potential function [4]. The direction of plastic flow of each failure mode can be written as;

• plastic flow of fibre damage (tension or compression)

$$\left(\frac{\partial F_s}{\partial \pmb{\sigma}}\right)_{fibre} = \begin{bmatrix} \frac{\partial F_s}{\partial \sigma_{11}} \\ \frac{\partial F_s}{\partial \sigma_{22}} \\ \frac{\partial F_s}{\partial \sigma_{33}} \\ \frac{\partial F_s}{\partial \sigma_{12}} \\ \frac{\partial F_s}{\partial \sigma_{13}} \\ \frac{\partial F_s}{\partial \sigma_{23}} \end{bmatrix} = \begin{bmatrix} \frac{\partial F_s}{\partial \sigma_{11}} \\ 0 \\ 0 \\ 0 \\ 0 \\ 0 \end{bmatrix} \tag{43}$$

- plastic flow of matrix damage (tension or compression)

$$\left(\frac{\partial F_s}{\partial \boldsymbol{\sigma}}\right)_{matrix} = \begin{bmatrix} \dfrac{\partial F_s}{\partial \sigma_{11}} \\ \dfrac{\partial F_s}{\partial \sigma_{22}} \\ \dfrac{\partial F_s}{\partial \sigma_{33}} \\ \dfrac{\partial F_s}{\partial \sigma_{12}} \\ \dfrac{\partial F_s}{\partial \sigma_{13}} \\ \dfrac{\partial F_s}{\partial \sigma_{23}} \end{bmatrix} = \begin{bmatrix} 0 \\ \dfrac{\partial F_s}{\partial \sigma_{22}} \\ 0 \\ \dfrac{\partial F_s}{\partial \sigma_{12}} \\ 0 \\ 0 \end{bmatrix} \tag{44}$$

To calculate the plastic multiplier, the damage surface consistency condition is applied as;

$$\partial \mathscr{F}(\sigma, \Psi) = \frac{\partial \mathscr{F}(\sigma, \Psi)}{\partial \sigma} \bullet (\partial \sigma) + \frac{\partial \mathscr{F}(\sigma, \Psi)}{\partial \Psi} \bullet (\partial \Psi) = 0 \tag{45}$$

The incremental stress–strain equation can be derived based on Hooke's law in incremental form to relate the stress and elastic strains. The explicit incremental of the orthotropic material relationship can be written as:

$$\partial \sigma = C \bullet d\varepsilon^e = C(d\varepsilon - d\varepsilon^p) \tag{46}$$

Substituting the plastic strain in the above equation;

$$\partial \sigma = C \left(d\boldsymbol{\varepsilon} - d\lambda \frac{\partial F_s}{\partial \boldsymbol{\sigma}} \right) \tag{47}$$

This equation is substituted into the damage surface consistency condition as;

$$\frac{\partial \mathscr{F}(\sigma, \Psi)}{\partial \sigma} \bullet C \left(d\boldsymbol{\varepsilon} - d\lambda \frac{\partial F_s}{\partial \boldsymbol{\sigma}} \right) + \frac{\partial \mathscr{F}(\sigma, \Psi)}{\partial \Psi} \bullet (\partial \Psi) = 0 \tag{48}$$

Thus, the plastic multiplier can be obtained as;

$$d\lambda = \frac{\frac{\partial \mathscr{F}(\sigma, \Psi)}{\partial \sigma} \bullet C \bullet d\boldsymbol{\varepsilon} + \frac{\partial \mathscr{F}(\sigma, \Psi)}{\partial \Psi} \bullet (\partial \Psi)}{\frac{\partial \mathscr{F}(\sigma, \Psi)}{\partial \sigma} \bullet C \bullet \frac{\partial F_s}{\partial \boldsymbol{\sigma}}} \tag{49}$$

where C is the effective stiffness matrix, which can be written [3] as;

$$C = \begin{bmatrix} \dfrac{(1-\omega_{11})E_{11}(1-\nu_{23}\nu_{32})}{\Delta} & \dfrac{(1-\omega_{22})E_{22}(\nu_{12}-\nu_{13}\nu_{32})}{\Delta} & \dfrac{E_{33}(\nu_{13}-\nu_{12}\nu_{23})}{\Delta} & & & \\ \dfrac{(1-\omega_{11})E_{11}(\nu_{21}-\nu_{31}\nu_{23})}{\Delta} & \dfrac{(1-\omega_{22})E_{22}(1-\nu_{13}\nu_{31})}{\Delta} & \dfrac{E_{33}(\nu_{23}-\nu_{21}\nu_{13})}{\Delta} & & 0 & \\ \dfrac{(1-\omega_{11})E_{11}(\nu_{31}-\nu_{21}\nu_{32})}{\Delta} & \dfrac{(1-\omega_{22})E_{22}(\nu_{32}-\nu_{12}\nu_{31})}{\Delta} & \dfrac{E_{33}(1-\nu_{12}\nu_{21})}{\Delta} & & & \\ & & & (1-\omega_{12})G_{12} & 0 & 0 \\ & 0 & & 0 & (1-\omega_{13})G_{13} & 0 \\ & & & 0 & 0 & (1-\omega_{23})G_{23} \end{bmatrix} \tag{50}$$

$$\Delta = 1 - \nu_{12}\nu_{21} - \nu_{23}\nu_{32} - \nu_{31}\nu_{13} - 2\nu_{13}\nu_{21}\nu_{32}$$

and

$$\omega_{11} = \omega_{11}^t + \omega_{11}^c - \omega_{11}^t \omega_{11}^c$$

$$\omega_{22} = \omega_{22}^t + \omega_{22}^c - \omega_{22}^t \omega_{22}^c$$

The stress–strain constitutive relationship of the damage model is updated as;

Table 1
Carbon/epoxy properties [8].

Carbon/epoxy properties			
Longitudinal modulus E_1 (GPa)	93.7	Longitudinal tensile strength X_T (MPa)	1850
Transverse modulus E_2 & E_3 (GPa)	7.45	Longitudinal compressive strength X_C (MPa)	1470
Shear modulus G_{12}, G_{13}, G_{23} (GPa)	3.97	Transverse tensile strength Y_T (MPa)	30
Poisson's ratio v_{12}, v_{13}, v_{23}	0.261	Transverse compressive strength Y_C (MPa)	140
Density $\rho (\text{kg/m}^3)$	1600	Shear strength S (MPa)	80

$$\boldsymbol{\sigma} = C \cdot d\boldsymbol{\varepsilon}^e = C(\boldsymbol{\varepsilon} - \boldsymbol{\varepsilon}^p) \tag{51}$$

where

$$\boldsymbol{\sigma} = \begin{bmatrix} \sigma_{11} & \sigma_{22} & \sigma_{33} & \sigma_{12} & \sigma_{13} & \sigma_{23} \end{bmatrix}^T$$

$$\boldsymbol{\varepsilon} = \begin{bmatrix} \varepsilon_{11} & \varepsilon_{22} & \varepsilon_{33} & \varepsilon_{12} & \varepsilon_{13} & \varepsilon_{23} \end{bmatrix}^T$$

and

$$\boldsymbol{\varepsilon}^p = \begin{bmatrix} \varepsilon_{11}^p & \varepsilon_{22}^p & \varepsilon_{33}^p & \varepsilon_{12}^p & \varepsilon_{13}^p & \varepsilon_{23}^p \end{bmatrix}^T$$

5. Validation of proposed damage model

5.1. Impact test

Laminated composites have been widely adopted in load-bearing structures because they possess the necessary properties in terms of strength, stiffness, and fatigue resistance. In the most common scenario, the impact loads on the structures are in the through-thickness direction and can lead to serious damage, and this is considered an obstacle to the more widespread use of laminates. The energy released during loading is absorbed through a combination of damage such as intralaminar damage (matrix cracking), fibre breakage and fibre–matrix debonding. As a result, the capacity of composite laminates to carry a load will be significantly reduced when damage takes place. In some cases, such as high velocity impact (ballistic impacts), the damage can be seen by the naked eye. In other cases, especially when the structure is impacted by a low-velocity object, the defect develops internally and it is difficult to discern the damage by the naked eye or external inspection. This internal damage will directly affect the material properties and can lead to a growing but unnoticed degradation in stiffness, so that a consequent sudden failure of the mechanical parts and a catastrophe could happen. A series of experimental tests had been implemented by Aymerich and Priolo [1], both drop-weight and compression tests, in their investigation to examine the behaviour of cross-ply graphite/epoxy laminates subjected to low-velocity impact. The development of the damage in the laminates structure, impact energy, released energy and post-impact behaviour were investigated. They used different, complementary observation techniques e.g. X-radiography, ultrasonic inspection, optical microscopy, and visual observation to identify internal damage propagation phenomena. Panels of cross-ply sequences $[0_3/90_3]_s$ were used in their experiments with average thickness of the cured panels 2.0 mm. The experiments were carried out using a drop weight testing machine, with rectangular plate of dimensions 65 mm × 87.5 mm, and hemispherical ended impactor 12.5 mm diameter and mass 2.28 kg. To measure the impact velocity of the impactor, an infra-red sensor was employed, and a strain-gauge bridge to measure the contact force between indenter and specimen.

5.1.1. Simulation model

In this section, the impact tests performed by Aymerich and Priolo [1] are modelled to validate the new approach to a damage evolution law and incremental constitutive relationship for intralaminar damage whether matrix or fibre. The developed models were coded and then implemented in finite element software. The model was divided into three sub-laminates, the thicknesses of the uppermost and lowermost sub-laminates were 0.666 mm with 0^0 fibre orientations, and each was connected to the mid layer (90^0 fibre orientations and 1.332 mm thick) by a cohesive element. The properties of the graphite/epoxy prepreg are presented in Table 1. It is necessary to update the plastic stresses and strains at each iteration, and a sequence of time steps $(t_n, t_{n+1}, t_{n+2}, \cdots)$ have been used for discrete iterative solutions. The incremental plastic constitutive model of stress is $\sigma_{n+1} = C(\varepsilon_{n+1} - \varepsilon_{n+1}^p)$ and incremental plastic strain can be updated as $\varepsilon_{n+1}^p = \varepsilon_n^p + \Delta\varepsilon_{n+1}^p$. The developed numerical model has been investigated for two impact energies 1.0 J and 12.5 J and the simulation findings which are in terms of the impact responses, damage propagation, matrix cracking and delamination interface behaviour are compared with experimental data available in the literature. Transverse matrix damage initially evolves in the layer with fibre orientation of 0^0, at the bottom of the laminate sequence, see Figs. 7 and 8, for results obtained experimentally by Aymerich and Priolo [1].

The tensile matrix cracking occurs due to tension stress in the lowermost layer, subsequently the damage develops upward into the other plies (middle and uppermost). Fig. 6 illustrates the tensile matrix crack in the lowermost layer and shear matrix cracks in the 90^0 plies when the specimen was impacted by 1.0 J energy. Fig. 6 also presents the simulation results based on the new damage evaluation
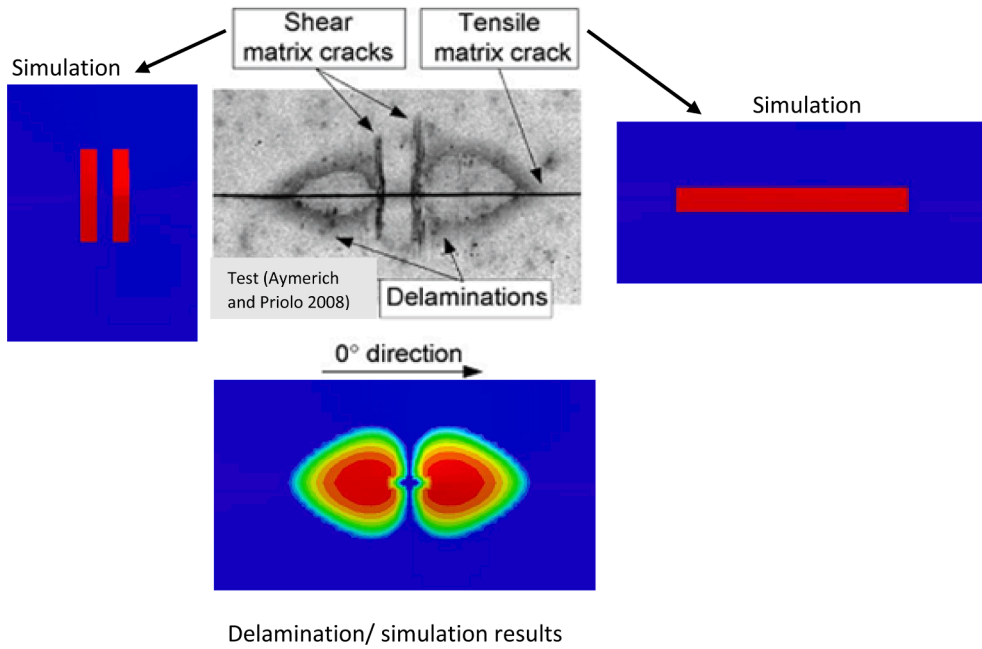
Fig. 6. Matrix cracking and delamination compared with experimental data (impact energy 1.0 J).
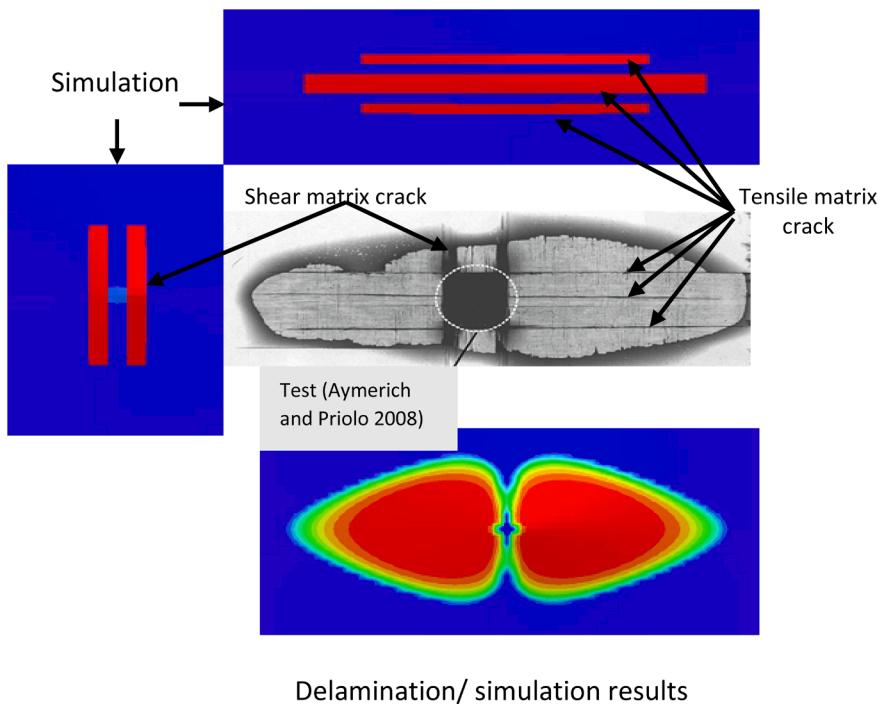

Fig. 7. Matrix cracking and delamination compared with experimental data (impact energy 12.5 J).

law and incremental damage constitutive relationship. It can be seen that the transverse matrix tension damage obtained from simulation is almost identical with the X-radiographs of the impact damage. As the damage moves upwards into the middle layer with fibre orientation of 90^0, the matrix cracking propagates along 90^0 plies. The same behaviour for damage growth was observed in the middle layer for both simulated and experimental results. Another type of damage was diagnosed at the interface between bottom and middle layers, this failure is known as interface delamination and it propagates in the same direction as the fibres in the bottom layer (0^0 fibre orientation), see Fig. 6.
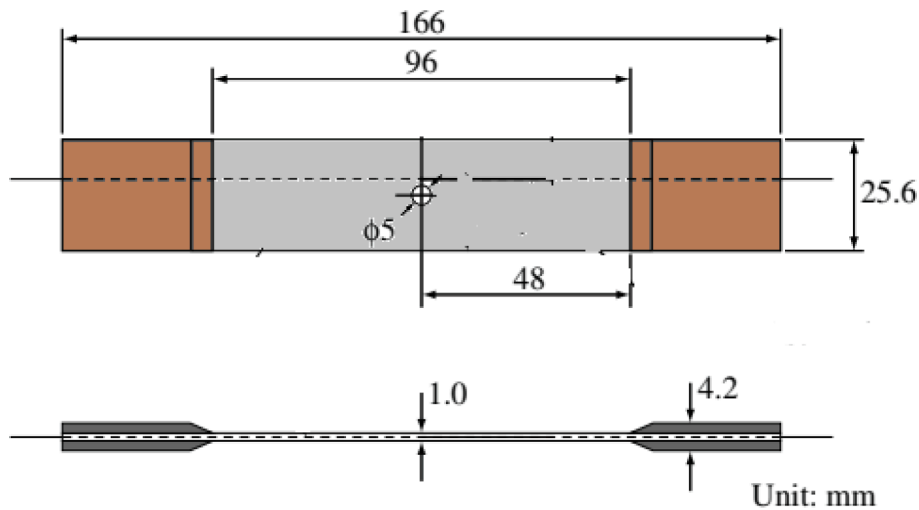
Fig. 8. Dimensions CFRP specimen [31].

With an impact energy of 12.5 J, the tensile matrix crack is seen as three lines parallel to the 0^0 fibre orientation, see Fig. 7. The experimental data was that obtained by Aymerich and Priolo [1]. Due to the greater impact force and enlarged contact area between indenter and specimen we see additional shear matrix cracks in the middle layer. The experimental evidence showed two separate delaminated areas propagating as lobes along tensile and shear matrix cracks. In the simulation, it can be seen that the process zones of damage congregate around matrix cracks in both 90^0 and 0^0 plies to produce the delamination lobes. The damage at the interface will take place when the damage parameter reaches unity.

If the process zone is removed from the output solution the distance between lobes observed in experimental data will also be seen in numerical model, as seen in Fig. 7. Therefore, the developed model of impact damage has the ability to simulate damage behaviour very similar to that observed in the X-radiographs obtained by Aymerich and Priolo [1].

5.2. Open hole tension model

In this section, the tension tests of the holed specimen performed by Yashiro et al. [31] are modelled to validate the new approach of composite materials under tensile load. Yashiro et al. [31] used CFRP cross-ply laminate (T800H/3631) with stacking configuration $[0_2/90_2]_S$. The specimen was rectangular in shape with a hole (diameter = 5 mm) at the centre. The dimensions of the specimen are illustrated in Fig. 8.

Quasi-static tensile tests were carried out by Yashiro et al. [31] using a universal electromechanical system with a cross-head speed of 0.25 mm/min. Different types of damage can be seen in the experiment test using soft X-ray radiography. The X-ray image obtained by Yashiro et al. [31] as shown in Fig. 9. The transverse cracks are clearly observed at (90^0 ply), and its number increase when the applied load increased.

The holed cross-ply laminate model was divided into two sub-laminates (0^0 fibre orientations and 90^0 fibre orientations of plies) with thicknesses of the each layer was 0. 0.25 mm thick. Due to the symmetry of the holed specimen, only a quarter model was performed in finite element software to reduce the time-consuming to analyse the model. The simulation results of the specimen under tension load are illustrated in Fig. 10. It is clearly seen that the damaged region spread (transverse cracks) increased at (90^0 ply) when the applied load increased, this is similar to that presented in the X-ray image. This confirms the validity of the new approach to a damage evolution law for intra-laminar damage.

6. Conclusions

Severe environmental conditions including both low-velocity and high-velocity impacts, can cause damages in composite materials. Damage in laminated composites affects mechanical properties (e.g. stiffness degradation) of the composite structure. The developed model based on a computational algorithm was successful in predicting consequential damage and thus, can save hugely in time and money when used to assess the integrity of large structures.

A three-dimensional intralaminar damage model has been developed and implemented in finite element software. Impact response of laminates subjected to impact energies 1.0 J and 12.5 J, has been quantified using the developed approach for predicting intralaminar damage. The observed matrix cracking features, and delamination damage area are discussed. Obtained results have been verified by comparison with experimental tests. It is clearly observed that the maximum central displacement and behaviour response when using the proposed model are very similar to the experimental findings reported in the literature. Also, the results showed that the use of plastic damage model gives consistent results for both all impact energies tested.
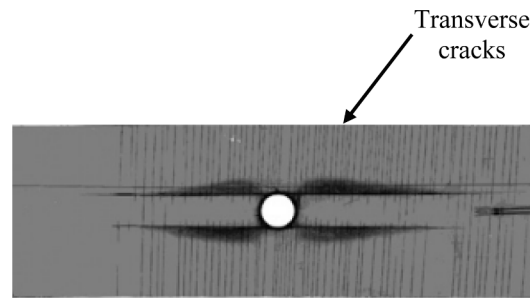
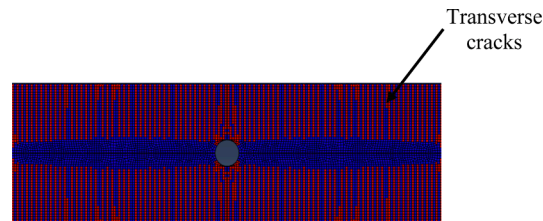**Fig. 9.** X-ray images obtained in the experiment by [31].

Fig. 10. Transverse cracks at 90^0 ply using proposed damage model.

CRediT authorship contribution statement

Ghalib R. Ibrahim: Investigation, Formal analysis, Methodology, Software, Writing – original draft, Writing – review & editing, Validation. **A. Albarbar:** Supervision, Resources. **Khaldoon F. Brethee:** Resources, Software.

Declaration of Competing Interest

The authors declare that they have no known competing financial interests or personal relationships that could have appeared to influence the work reported in this paper.

References

[1] Aymerich F, Priolo P. Characterization of fracture modes in stitched and unstitched cross-ply laminates subjected to low-velocity impact and compression after impact loading. Int J Impact Eng 2008;35(7):591–608.
[2] Davila CG, Camanho PP, Rose CA. Failure criteria for FRP laminates. J Compos Mater 2005;39(4):323–45.
[3] Donadon MV, Iannucci L, Falzon BG, Hodgkinson JM, de Almeida SFM. A progressive failure model for composite laminates subjected to low velocity impact damage. Comput Struct 2008;86(11–12):1232–52.
[4] Dunne F, Petrinic N. Introduction to computational plasticity. Oxford University Press on Demand; 2005.
[5] Fagan EM, Kennedy CR, Leen SB, Goggins J. Damage mechanics based design methodology for tidal current turbine composite blades. Renew Energy 2016;97: 358–72.
[6] Fakoor M, Ghoreishi S Mohammad Navid. Experimental and numerical investigation of progressive damage in composite laminates based on continuum damage mechanics. Polym Test 2018;70:533–43.
[7] Feng D, Aymerich F. Finite element modelling of damage induced by low-velocity impact on composite laminates. Compos Struct 2014;108:161–71.
[8] Hameed MA, Ibrahim GR, Albarbar A. Effect of friction and shear strength enhancement on delamination prediction. J Compos Mater 2020;54(23):3329–42.
[9] Haselbach PU, Bitsche RD, Branner K. The effect of delaminations on local buckling in wind turbine blades. Renew Energy 2016;85:295–305.
[10] Hashin Z. Failure criteria for unidirectional fiber composites. J Appl Mech-Trans ASME 1980;47(2):329–34.
[11] Hashin Z, Rotem A. Fatigue failure criterion for fiber reinforced materials. J Compos Mater 1973;7(Oct):448–64.
[12] Hinton MJ, Kaddour AS, Soden PD. A comparison of the predictive capabilities of current failure theories for composite laminates, judged against experimental evidence. Compos Sci Technol 2002;62(12–13):1725–97.
[13] Ibrahim GR, Albarbar A. A new approach to the cohesive zone model that includes thermal effects. Compos B Eng 2019;167:370–6.
[14] Ibrahim GR, Albarbar A, Brethee KF. Progressive failure mechanism of laminated composites under fatigue loading. J Compos Mater 2020;55(1):137–44.
[15] Jiang W, Yao W, Qi W, Shen H. Study on the fractal dimension and evolution of matrix crack in cross-ply GFRP laminates. Theor Appl Fract Mech 2020;107: 102478. https://doi.org/10.1016/j.tafmec.2020.102478.
[16] Liao BB, Liu PF. Finite element analysis of dynamic progressive failure of plastic composite laminates under low velocity impact. Compos Struct 2017;159: 567–78.
[17] Liu PF, Liao BB, Jia LY, Peng XQ. Finite element analysis of dynamic progressive failure of carbon fiber composite laminates under low velocity impact. Compos Struct 2016;149:408–22.
[18] Namdar Ö, Darendeliler H. Buckling, postbuckling and progressive failure analyses of composite laminated plates under compressive loading. Compos B Eng 2017;120:143–51.
[19] Puck A, Schürmann H. Failure analysis of FRP laminates by means of physically based phenomenological models. Compos Sci Technol 2002;62(12–13): 1633–62.
[20] Rivallant S, Bouvet C, Hongkarnjanakul N. Failure analysis of CFRP laminates subjected to compression after impact: FE simulation using discrete interface elements. Compos Part a-Appl Sci Manuf 2013;55:83–93.

[21] Shi Y, Swait T, Soutis C. Modelling damage evolution in composite laminates subjected to low velocity impact. Compos Struct 2012;94(9):2902–13.

[22] Shor O, Vaziri R. Application of the local cohesive zone method to numerical simulation of composite structures under impact loading. Int J Impact Eng 2017; 104:127–49.

[23] Sridharan S, Pankow M. Performance evaluation of two progressive damage models for composite laminates under various speed impact loading. Int J Impact Eng 2020;143:103615. https://doi.org/10.1016/j.ijimpeng.2020.103615.

[24] Sun CT, Quinn BJ, Oplinger DW. Comparative evaluation of failure analysis methods for composite laminates; 1996.

[25] Tan R, Xu J, Sun W, Liu Z, Guan Z, Guo X. Relationship between matrix cracking and delamination in CFRP cross-ply laminates subjected to low velocity impact. Materials 2019;12(23):3990.

[26] Tarfaoui M, El Moumen A, Lafdi K. Progressive damage modeling in carbon fibers/carbon nanotubes reinforced polymer composites. Compos B Eng 2017;112: 185–95.

[27] Turon A, Costa J, Camanho PP, Dávila CG. Simulation of delamination in composites under high-cycle fatigue. Compos Part a-Appl Sci Manuf 2007;38(11): 2270–82.

[28] Verma AS, Vedvik NP, Gao Z. A comprehensive numerical investigation of the impact behaviour of an offshore wind turbine blade due to impact loads during installation. Ocean Eng 2019;172:127–45.

[29] Wu Z, Shi L, Cheng X, Xiang Z, Hu X. Transverse impact behavior and residual axial compression characteristics of braided composite tubes: experimental and numerical study. Int J Impact Eng 2020;142:103578. https://doi.org/10.1016/j.ijimpeng.2020.103578.

[30] Yang W, Court R, Jiang J. Wind turbine condition monitoring by the approach of SCADA data analysis. Renew Energy 2013;53:365–76.

[31] Yashiro S, Okabe T, Toyama N, Takeda N. Monitoring damage in holed CFRP laminates using embedded chirped FBG sensors. Int J Solids Struct 2007;44(2): 603–13.

[32] Zuo Y, Montesano J, Singh CV. Assessing progressive failure in long wind turbine blades under quasi-static and cyclic loads. Renew Energy 2018;119:754–66.